

AEGIS: INFRARED SPECTRAL ENERGY DISTRIBUTIONS OF MIPS 70 μ M SELECTED SOURCES

M. SYMEONIDIS,¹ D. RIGOPOULOU,¹ J.-S. HUANG,² M. DAVIS,³ M. L. N. ASHBY,² P. BARMBY,² E. EGAMI,⁴ G. G. FAZIO,² E. LEFLOC'H,⁴ G. RIEKE,⁴ S. P. WILLNER,² G. WILSON,⁵

Draft version September 7, 2018

ABSTRACT

We present 0.5 – 160 μ m Spectral Energy Distributions (SEDs) of galaxies, detected at 70 μ m with the Multiband Imaging Photometer for Spitzer (MIPS), using broadband imaging data from Spitzer and ground-based telescopes. Spectroscopic redshifts, in the range $0.2 \leq z \leq 1.5$, have been measured as part of the Deep Extragalactic Evolutionary Probe2 (DEEP2) project. Based on the SEDs we explore the nature and physical properties of the sources. Using the optical spectra we derive H_{β} and [OII]-based Star Formation Rates (SFR) which are 10–100 times lower than SFR estimates based on IR and radio. The median offset in SFR between optical and IR is reduced by a factor of ~ 3 when we apply a typical extinction corrections. We investigate mid-to-far infrared correlations for low redshift (>0.5) and high redshift ($0.5 < z < 1.2$) bins. Using this unique “far-infrared” selected sample we derive an empirical mid to far-infrared relationship that can be used to estimate the infrared energy budget of galaxies in the high-redshift universe. Our sample can be used as a template to translate far-infrared luminosities into bolometric luminosities for high redshift objects.

Subject headings: infrared: galaxies — galaxies: fundamental parameters (classification, colors, luminosities)— galaxies: high-redshift

1. INTRODUCTION

The first breakthrough in infrared astronomy followed the launch of the Infrared Astronomical Satellite (IRAS), which uncovered a substantial population of galaxies very luminous in the infrared (e.g. Neugebauer et al. 1984, Soifer et al. 1987). Its successor, the Infrared Space Observatory (ISO), demonstrated that a significant fraction of the energy budget in star-forming galaxies emerges in the infrared regime (e.g Soifer et al. 1984). Since then, attempts to describe the nature of these objects have lead to extensive studies of the properties of dust and its presence in star forming regions, using Spectral Energy Distributions (SEDs) and infrared colors as parameter constraints (e.g. Rowan-Robinson & Crawford 1989, Dale & Helou 2002). At the same time, correlations using photometry at different wavelengths have proved extremely useful in facilitating the study of the high- z universe and compensating for lack of long wavelength InfraRed (IR) data (e.g. Sanders & Mirabel 1996).

Since the launch of the Spitzer Space Telescope (SST) (Werner et al. 2004), we are able to study the emission from interstellar dust across a wide range of environments both locally and at high redshifts. Deep surveys with the InfraRed Array Camera (IRAC) and the Multiband Imaging Photometer for Spitzer (MIPS) (Rieke et al. 2004) have provided a wealth of energy distributions at every redshift. This letter presents the

analysis of a sample of high-redshift sources detected at 70 μ m by MIPS, in the region of the Extended Groth Strip (EGS). We have used a multitude of photometry in the near, mid and far infrared to construct SEDs and examine galaxy colours and have demonstrated the compatibility of this population with samples of local infrared luminous galaxies.

2. THE OBSERVATIONS

The All-Wavelength Extended Groth Strip International Survey (AEGIS) is a multi-Wavelength survey with a coverage of $2.0^{\circ} \times 10'$ (Davis et al. 2006). MIPS observations of the Extended Groth Strip were conducted in two epochs: January and June of 2004. The effective EGS area with both IRAC and MIPS coverage is 725 arcsec². 180 70 μ m sources were detected in this region with a point source sensitivity of 4 mJy at 5σ , hereafter the MIPS 70 μ m sample.

The IRAC and MIPS Basic Calibrated Data (BCD) delivered by the Spitzer Science Center (SSC) included flat-field and linearity corrections, dark subtraction and flux calibration. The BCD data were further processed by each team’s own refinement routines, including distortion corrections, pointing refinement, mosaicing and cosmic ray removal by sigma-clipping. We used DAOPHOT to extract sources from both IRAC and MIPS images; a Point Spread Function (PSF) FWHM of 1.8”–2.0” for IRAC and 35”/40” for MIPS 70/160 μ m was used. The aperture fluxes in each band were subsequently corrected to total fluxes using known PSF growth curves from Fazio et al. (2004), Huang et al. (2004).

All 70 μ m sources in the sample are detected at the IRAC 3.6, 4.5, 5.8, 8.0 μ m, and MIPS 24 μ m bands. However, because of the different alignment of the MIPS and IRAC images we do not have IRAC fluxes for all 70 μ m sources. 88% of sources in the sample are also detected at 160 μ m. In addition, the AEGIS data set (Davis et al. 2006) provides multi-wavelength photometry and

¹ Astrophysics Department, Oxford University, Oxford OX1 3RH

² Harvard-Smithsonian Ctr. for Astrophysics, 60 Garden St., Cambridge, MA 02138

³ Dept. of Astron., Univ. of California Berkeley, Campbell Hall, Berkeley, CA 94720

⁴ Steward Observatory, University of Arizona, 933 N. Cherry Avenue Tucson, AZ 85721

⁵ Spitzer Science Ctr., California Inst. of Technology, 1200E California Blvd., Pasadena, CA 91125

spectroscopic redshifts for the $70\mu\text{m}$ sample, which permit the study of their X-ray-to-radio SEDs. 42 sources in the $70\mu\text{m}$ population have a reliable DEEP2 spectroscopic redshift in the range of $0 < z < 1.2$ (we only use redshifts with qualities 3 or 4, according to the DEEP2 classification). We further divide the $70\mu\text{m}$ sources in two redshift bins: $z \leq 0.5$ and $0.5 < z < 1.2$ (the terms “low” and “high” redshift hereafter). Although, the DEEP2 project uses colour criteria to preselect objects with photometric redshifts in the range 0.7-1.55, these constraints have not been imposed on the EGS, therefore our redshift sample is not biased against the $70\mu\text{m}$ sample. We limit the analysis in this letter to 38 objects for which we have full visible-IR SEDs and reliable (see above) spectroscopic redshifts (the remaining 4 objects do not have full SED coverage).

3. PROPERTIES OF THE $70\mu\text{m}$ POPULATION

3.1. Spectral Energy Distributions

Using CFHT B,R,I imaging data and Spitzer photometry (3.6, 4.5, 5.8, 8.0, 24, 70 and $160\mu\text{m}$) we were able to construct 96 full SEDs, with 38 having reliable spectroscopic redshifts. The SEDs of all objects with reliable spectroscopic redshifts (38 sources) are shown in Figure 1. We group the SEDs in three panels: objects with low- z (left), high- z (middle) and, a separate panel for objects with AGN-like SEDs (right).

Objects from the low/high- z groups show typical galaxy SEDs: the optical bands are dominated by starlight which is then thermally reprocessed by dust and re-emitted at longer wavelengths, giving rise to the noticeable increase in Mid-InfraRed (MIR) flux. It is not surprising that the optical/near-IR part of the high- z SEDs is almost an order of magnitude lower than the low- z equivalent, as it samples a shorter wavelength region more strongly affected by extinction.

In the mid-infrared regime (ie. $12 < \lambda < 24\mu\text{m}$) we find that the high- z objects have overall much higher flux densities than the low- z objects. There are two explanations for this: either high- z sources have higher hot dust emission shortwards of $20\mu\text{m}$ or, low- z sources have higher cold dust emission longwards of $60\mu\text{m}$. Low- z objects show a predominant excess flux in the IRAC $8\mu\text{m}$ band, which we attribute to emission at 6.2 and/or $7.7\mu\text{m}$, from Polycyclic Aromatic Hydrocarbons (PAHs).

In the far-infrared we note a large scatter in $160\mu\text{m}$ fluxes evident in both low and high- z sources. We find $70\mu\text{m}/160\mu\text{m} \nu f_\nu$ ratios of ~ 1 and ~ 0.4 for the low and high- z sources, respectively. This is in agreement with the energy distributions of local HII region-like galaxies (e.g. Dale et al. 2005, hereafter D05). In the Spitzer Infrared Nearby Galaxy Survey (SINGS) results, presented in D05, approximately 35% of the objects show a turnover at $160\mu\text{m}$ and their average $70/160 \nu f_\nu$ ratios are ~ 1 ; accordingly, we evaluate our objects to be equally “warm” to local sources.

Overall, the majority of our objects have characteristics consistent with those of luminous star-forming infrared galaxies. However, a small fraction (9 out of 96) reveal power-law type SEDs indicative of the presence of an Active Galactic Nucleus (AGN) (of the 9 AGN-candidates only 3 have secure DEEP2 spectroscopic redshifts). These power law-type sources have distinctly redder IRAC colors and are clearly identified in IRAC-color

plots. Interestingly, the available optical spectra do not show any of the characteristic signatures of an AGN, such as broad wings in the Balmer/Oxygen lines; it is only with the addition of MIR data that we are able to peer through the obscuring dust and reveal the active nucleus. Only 1/3 of these candidate-AGNs are also detected in the x-rays, not surprising, as the Chandra full band (0.5-10 keV) data (flux limit 3.5×10^{-15} ergs/s/cm²) (Georgakakis et al. 2006) are not as deep as the MIPS and IRAC detections. The selected fraction of power law-type galaxies agrees with a similar study in Frayer et al. (2006). However, taking into account ultra-hard (5-10 keV) x-ray fluxes and hardness ratios leads us to an upper limit of 15% of AGNs in the sample, consistent with the findings of Fadda et al. (2002), Franceschini et al. (2003). Brandt et al. (2006), show that in their $24\mu\text{m}$ survey the contribution of AGNs is high ($> 40\%$) when selecting the brightest $z > 0.6$ sources, but $\sim 10\%$ when considering the whole redshift range. Our results are consistent with this study, as our power law-type sources with spectroscopic redshifts are found at $z > 0.6$.

3.2. Star Formation Rates

In this section we carry out a comparative study of different diagnostics in order to trace the Star Formation Rate (SFR) in our sample. Such a study is possible given the wealth of information available for the AEGIS project (Davis et al. 2006). We derive SFRs based on optical Balmer/[OII] emission lines, IR (present work) and 20 cm radio (Ivison et al. 2006) luminosities. Our computations are based on the prescriptions of Kennicutt (1998) and Bressan, Silva & Granato (2002).

All available spectra were examined for the presence of hydrogen recombination and oxygen forbidden emission lines, as tracers of young stellar populations. We identified H β and [OII] features in 22% and 10% of the spectra, respectively. We extracted line fluxes by calibrating the continuum using CFHT optical/near-IR data and included stellar absorption corrections for each Balmer line. We derive an “average” SFR_{opt} of $2 M_\odot/\text{yr}$. Likewise we derived average SFR_{IR} and SFR_{radio} of 100 and $80 M_\odot/\text{yr}$, respectively.

In Figure 2 we show a comparison of optical vs IR vs radio SFRs as a function of redshift for 38 objects from the $70\mu\text{m}$ sample, which have full IRAC and MIPS photometry as well as reliable spectroscopic redshifts in the range $0 < z < 1.2$. Radio and IR SFRs reach values of $\sim 900 M_\odot/\text{yr}$, revealing an active star-forming population. The SFR_{IR} is on average 50 times higher than the non-extinction-corrected SFR_{opt} . Assuming an $A_V \sim 2$ (a typical A_V value for infrared selected objects, see e.g. Rigopoulou et al. 2000) then $\text{SFR}_{IR}/\text{SFR}_{optical} \sim 10$ confirming that extinction is indeed very high. The fact that $\text{SFR}_{IR} \sim \text{SFR}_{radio}$ reinforces the notion that the $70\mu\text{m}$ population is indeed made up of dusty star-forming galaxies. Moreover, it provides a nice confirmation that the radio-far-IR correlation that was found to exist for local galaxies (e.g. Condon, Anderson & Helou, 1991) extends out to $z \sim 1$ sources. Finally, it is important to stress that any attempts to derive SFR estimates based on optical/UV measurements are likely to provide severe underestimates.

4. THE MID-TO-FAR INFRARED CORRELATION

In this section we investigate the mid-to-far infrared luminosity correlations. We limit our study to objects with confirmed spectroscopic redshifts and full SEDs, and explore the correlations for each redshift bin separately. For our computations we have adopted a cosmology with $\Omega_M=0.3$, $\Omega_\Lambda=0.7$ and $H_0 = 71 \text{ km.sec}^{-1} \text{ Mpc}^{-1}$. Investigation of spectral energy distributions and behavior of colors (see earlier text) has lead us to the conclusion that our $70\mu\text{m}$ sample shares many similar characteristics with local infrared luminous galaxies. Consequently to estimate K-corrections we used the complete SED of the local galaxy NGC 4631 (convolved to the Spitzer resolution) and followed the prescription of Hogg (2002). We are, of course, aware that use of a single template to derive K-corrections may introduce some biases. However, as Appleton et al. (2004) also points out the presently available models do not fully encompass the observed parameters especially in the far-infrared. This is likely to change with the availability of more Spitzer far-infrared datasets such as SINGS.

In Figure 3 we plot the 24 vs 70 and 70 vs 160 μm correlations. We have performed a weighted least-square fit for each case, taking into account the calibration errors of 10 and 20% for the 24 and $70\mu\text{m}$ fluxes respectively, as well as the errors arising from SED fitting. We quantified the strength of the correlations using the Pearson linear coefficient. The Pearson coefficient ranges between 0 and |1| for no or excellent correlation respectively, with any intermediate value indicating the degree of linear dependence between the variables. Our values of ~ 0.8 for the 24– $70\mu\text{m}$ plot and ~ 0.9 for the 70– $160\mu\text{m}$ plot indicate a strong relation.

As expected, most of the energy in this population

is emitted in the far-IR, also supported by the lines of best fit. By combining the above results we derived a relationship to estimate the monochromatic luminosity at $160\mu\text{m}$ from data at 24 and $70\mu\text{m}$, with an accuracy higher than 30%, for the low- z and high- z cases.

$$\text{For } z \leq 0.5 : \quad L_{160} \sim 0.9L_{24} + 0.8L_{70} \quad (L_\odot) \quad (1)$$

$$\text{For } z > 0.5 : \quad L_{160} \sim 0.6L_{24} + 0.4L_{70} \quad (L_\odot) \quad (2)$$

It is evident that the well-studied mid-to-far infrared relation found to hold for local galaxies (e.g. Dale & Helou 2002) can also be extended to the non-local universe. Although, by limiting our study to the objects with spectroscopic redshifts, we select in favor of the brightest sources, we still manage to sample a wide range of luminosities representative of $z \sim 1$ populations emerging through various deep infrared surveys. The correlations we have found can be used to obtain a direct estimate of the far-infrared luminosity of $z \sim 1$ objects and avoid the large errors introduced from MID-FIR extrapolations of various galaxy templates.

MS has been supported by a Marie Curie Excellence Grant while working on this project MEXT-CT-2003-002792. DR acknowledges support from the Leverhulme Trust via a Research Fellowship. This work is based on observations made with the Spitzer Space Telescope, which is operated by the Jet Propulsion Laboratory, California Institute of Technology under NASA contract 1407. Support for this work was provided by NASA through Contract Number 1256790 issued by JPL.

REFERENCES

- Brand, K., et al., 2006, ApJ, 644, 143
 Bressan, A., Silva, L. & Granato, G., L., 2002, A&A, 392, 377-391
 Cram, L., et al., 1998, ApJ, 507, 155-160
 Coil, A., L., 2004, ApJ, 617, 765
 Dale, D.A., & Helou, G., 2002, ApJ, 576, 159
 Dale, D.A., Bendo, G.J., Engelbracht, C.W., Gordon, K.D., et al., 2005, ApJ, 633, 857
 Fadda, D., et al., 2002, A&A, 383, 838
 Fazio, G.G., Ashby, M.L.N. et al., 2004, ApJS, 154
 Franceschini, A., Berta, S., Rigopoulou, D., Aussel, H., et al., 2003, A&A, 403, 501
 Frayer, D., T., et al., 2006, AJ, 131, 250
 Genzel, R., Lutz, D., Sturm, E., Egami, E., 1998, ApJ, 498, 579
 Georgakakis, A., et al., 2006, in press
 Hogg, D., et al. 2002, astro-ph/0210394
 Huang, J-S., et al., 2004, ApJS, 154, 44
 Kennicutt, R., C., 1998, ApJ, 272, 54-67
 Neugebauer, G., et al., 1984, ApJ, 278, 1
 Poggianti, B., M., Bressan, A., & Franceschini, A., 2001, ApJ, 550, 195-203
 Puget, J.L., Lagache, G., Clements, D.L., Reach, W.T., et al., 1999, A&A, 345, 29
 Rieke, G.H., Young, E.T., et al., 2004, ApJS, 154, 45
 Rigopoulou, D., Spoon, H., W.W., Genzel, R., et al., 1999 AJ, 118, 2625
 Rigopoulou, D., et al., 2000, ApJ, 537, L85-L89
 Rowan-Robinson, M., & Crawford, J., 1989, MNRAS, 238, 523-558
 Sanders D. E. & Mirabel I. F., 1996, ARA&A, 34, 749
 Soifer, B.T., Rowan-Robinson, M., Houck, J.R., de Jong, T., et al., ApJ, 1984, 278, 71
 Soifer, B.T., et al., 1987, ARA&A, 25, 187
 Werner, M.W., Roellig, T.L., et al. 2004, ApJS, 254, 33

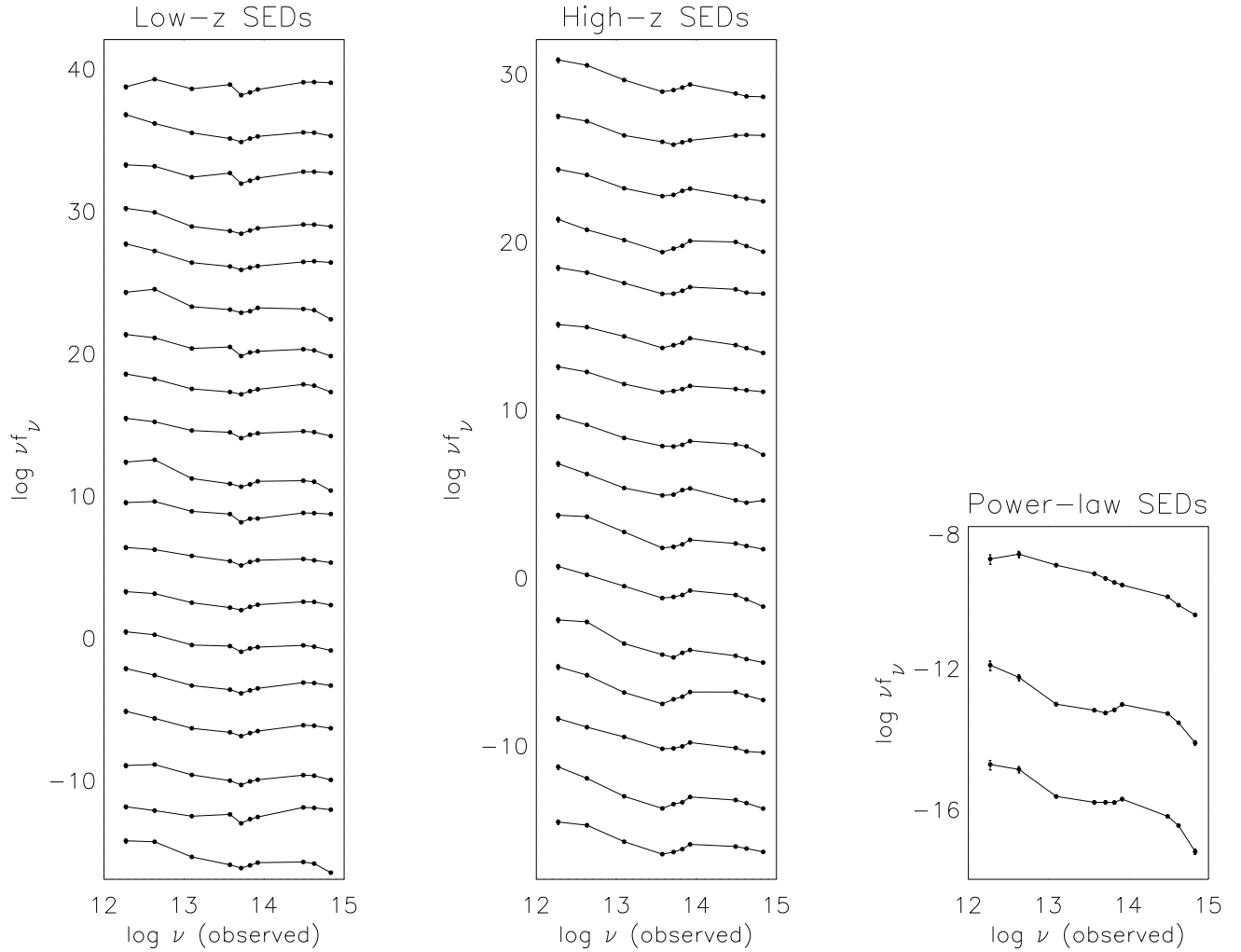


FIG. 1.— Full SEDs for the entire MIPS 70 μm sample with confirmed spectroscopic redshifts grouped into low-z (left), high-z (middle) and power-law (right) panels. The lower SED in each panel is in real y-axis units - for clarity, each subsequent SED in the low-z and power-law groups is transposed by 3 dex; in the high-z group the SEDs are transposed by 2 dex. In the direction of decreasing frequency, the 10 point photometry used to assemble the SEDs is: B, R, I magnitudes from CFHT, 3.6, 4.5, 5.8, 8 μm fluxes from IRAC and 24, 70, 160 μm fluxes from MIPS

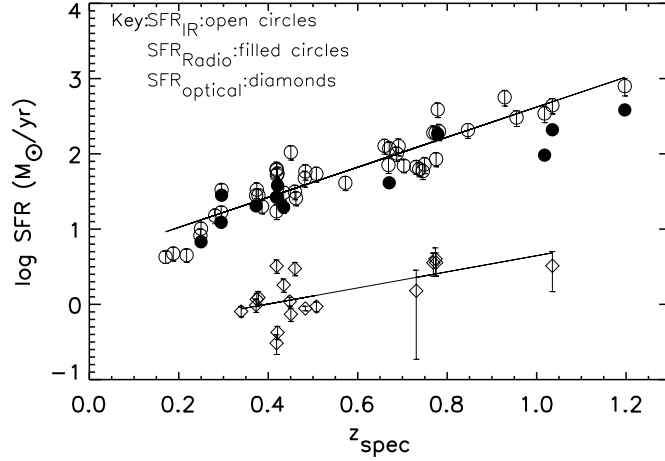


FIG. 2.— Plot of various indicators of the Star Formation Rate (SFR) as a function of redshift. SFRs estimated based on optical (H_β and [OII]) emission lines (open diamonds), radio (filled circles) and IR (open circles) luminosities. The line-fits represent the mean SFR_{IR} and SFR_{opt} .

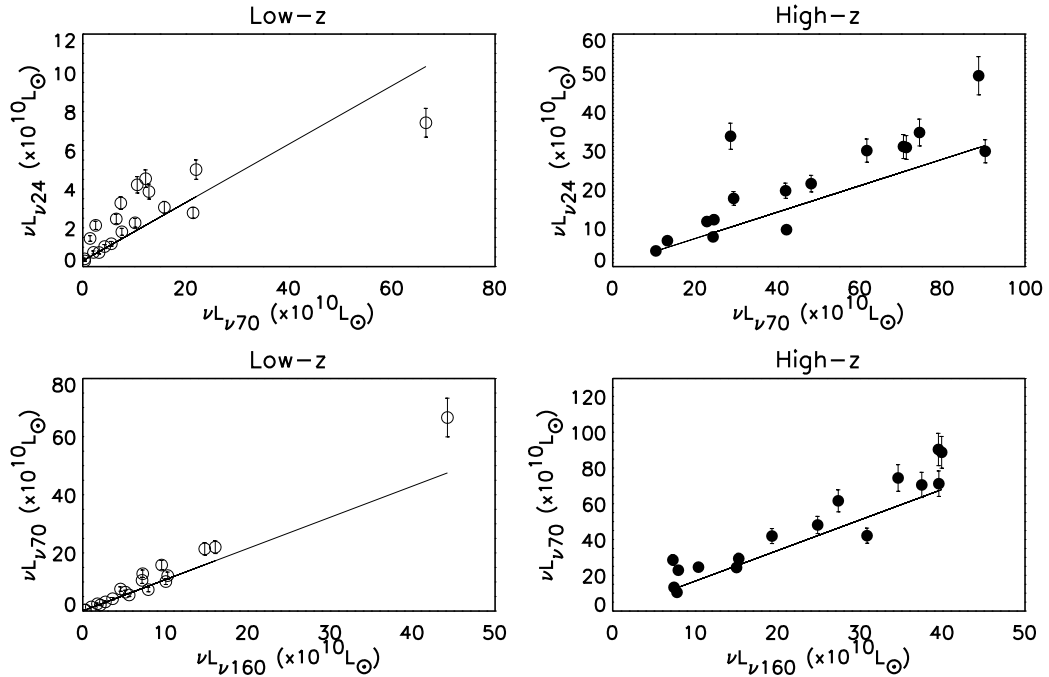


FIG. 3.— Linear Mid-to-far infrared L_{24} vs L_{70} and L_{70} vs L_{160} luminosity correlations for the objects with spectroscopic redshifts. The two redshift bins are $z \leq 0.5$ (open symbols, left) and $z > 0.5$ (filled symbols, right). $\nu L_{\nu\lambda}$ represents the monochromatic luminosity of the objects at wavelength λ . The least square fit is shown for all four cases.